中部大学大学院客員教授　田中基彦

◆ Graetzel's Letter : "Sequential deposition as a route to high-performance perovskite-sensitized solar cells", Nature 2013 (London, UK).

シリコンに次ぎ有望である，ペロブスカイト色素増感の有機太陽電池セルについて論文を読む。ここでは，表題，アブストラクト，Figures，Tables を読み，そして本論に移る。Figure 1 に実験の結果である全体の写真，J-V 曲線，X 線回折図，Figure 2 は薄膜太陽電池セルの SEM（走査電子顕微鏡）写真，Figure 3 に J-V 曲線，効率。

英文を段落ごとに読み，日本語に訳を書いてゆく（普通は英語を読んでも，日本語には翻訳しない。）意味が分からない単語は辞書を引く習慣をつける。この PDF の最後には，大きな文字で表示するため，6 ページに分割している。Figure は解説の p.5, p.8, p.10 に収録している。

➢ Abstract（訳文は次ページにあるが，主語・述語が対でわかるように，緑色で示す）

Following pioneering work, solution-processable organic–inorganic hybrid perovskites—such as CH3NH3PbX3 (X= Cl, Br, I)—have attracted attention as light-harvesting materials for mesoscopic solar cells. So far, the perovskite pigment has been deposited in a single step onto mesoporous metal oxide films using a mixture of PbX2 and CH3NH3X in a common solvent. However, the uncontrolled precipitation of the perovskite produces large morphological variations, resulting in a wide spread of photovoltaic performance in the resulting devices, which hampers the prospects for practical applications. (1)

Here we describe a sequential deposition method for the formation of the perovskite pigment within the porous metal oxide film. PbI2 is first introduced from solution into a nanoporous titanium dioxide film and subsequently transformed into the perovskite by exposing it to a solution of CH3NH3I.

We find that the conversion occurs within the nanoporous host as soon as the two components come into contact, permitting much better control over the perovskite morphology than is possible with the previously employed route. (2)

Using this technique for the fabrication of solid-state mesoscopic solar cells greatly increases the reproducibility of their performance and allows us to achieve a power conversion efficiency of approximately 15 per cent (measured under standard AM1.5G test conditions on solar zenith angle, solar light intensity and cell temperature). This twostep method should provide new opportunities for the fabrication of solution-processed photovoltaic cells with unprecedented power conversion efficiencies and high stability equal to or even greater than those of today's best thin-film photovoltaic devices. (3)

➢ 第 1 ページ左列の単語（表題，アブストラクト）

sequential deposition 連続変性法
-> 意訳では「成膜法」らしいが，液体から固体へ「連続的に性質を変化させる」，のが趣旨。

high performance 高い効率
*pigment 色素
deposited に入れる
mesoscopic メソスケールの（ここでは **1 micron と 1 nm の中間規模を指している**）
metal oxide film 金属酸化物のフィルム
solvent 溶液
precipitation 沈殿物
produce 生じさせる
morphological variation 形態学上の変化
result in… を帰結する
photovoltaic performance 起電力の性能
***hamper** 邪魔する，阻害する
prospect 見込み
practical application 現実性の応用
porous metal oxide 多孔性の 金属酸化物
transformed 変形させた
*exposing をさらして

Here we **describe** a … を記述する
We find that… …であると分かる
conversion 転化が起きること
nanoporus host ナノ多孔質のホスト(原意は，宿主)
as soon as… come into contact 接触すると直ちに…
permitting much better control （コンマに続けて）よりよく制御が可能である
over the morphology **than is possible with** … …で可能な形態学以上に
previously employed route 以前使っていた方法
using this technique for… この方法を使うことで （これ一塊が主語である）
the **fabrication** of solid-state… ソリッドステート…の製作
greatly increases the reproducibility **of**… の再現性を**大きく改善する** （これが述語）
allows us to achieve a power conversion efficiency… パワー出力の効率を出すことを可能にする
solar zenith angle 天頂角
cell temperature （太陽電池）セルの温度

this two-step method should **provide**…
（4 行もあるが，主語と述語は 1 通り） この2ステップの方法は…を可能としている
unprecedented power conversion efficiency **前例のない**パワー変換効率
equal to or even greater than those of today's best thin-film photovoltaic devices
今と同じかそれ以上の最高の薄膜光電圧のデバイスを超えた

(訳文)

意味上は3つのパラグラフ構成になる。ただし一続きの文章であり，段落には分けないこと。（アブストラクトを複数の段落に分けて書く人がいるが，間違いである。必ず雑誌の Editor が直してくる） 文章ごとに，意味を考えて訳す。

それではアブストラクトを日本語で書くと，

先駆者の研究を引き継ぎ，CH3NH3PbX3（X は Cl, Br, I）を一例として，
有機と非有機系溶液プロセスであるペロブスカイトは，メソスコピック系の
太陽電池セルに向けた光を生みだす物質として注目されている。 Part (0)

今までは，ペロブスカイト色素の処理を， PbX2 と CH3NH3PbX3 の一般溶液として，
メソ多孔質の金属酸化物フィルムへ一度のステップで製造してきた。

しかし，ペロブスカイトの予測不能な析出は大きな形態の変動をもたらし，
結果としてデバイスにおける光起電力の広い幅となり，現実応用の確実さを
妨げるものだった。 Part (1)

ここでは，多孔質金属酸化物フィルムに対する，ペロブスカイト色素の形成についての
連続的変性法を記述する。

まず PbI2 を溶液からナノ多孔質 TiO2 フィルムに持ちこんで，そして CH3NH3I
溶液に触れさせペロブスカイトへ変換させる。

2つの成分が直接接した瞬間に，その変化はナノ多孔質ホストのなかに起き，
以前試したどんな方法よりもペロブスカイトの形を支配することが確実である。 Part (2)

固体物理メソスケールにおける太陽電池の製法に応用するこの方法は，
パフォーマンスの再現性を改良し，パワー変換効率が約 15%を記録する
非常に大きな改良となった（太陽天頂角，太陽光強度，温度について，
標準 AM1.5G テスト状態で）。

この2段階法（固体化）により，今まで最高であった薄膜光電デバイスを越えたパワー変換効率と
高い安定性をもつ溶液プロセス光電圧セルの製作において，新しい機会を与えることだろう。 Part (3)

Part(0) と Part(3) だけで，論文の意図が読者に伝わる書き方である。
意訳のところはあるが，その雰囲気が伝わっているだろうか？

➢ **第 1 ページ右列　英語と訳文**　ここから本論
初めに実験装置の概略を示している。主語と述語は短いが，それを説明する修飾は長い。

We prepared mesoporous TiO2 (anatase) films by spin-coating a solution of colloidal anatase particles onto a 30-nm-thick compact TiO2 layer.

The underlayer was deposited by aerosol spray pyrolysis on a transparent-conducting-oxide glass substrate acting as the electric front contact of the solar cell.

Lead iodide (PbI2) was then introduced into the TiO2 nanopores by spin−coating a 462 mg ml−1 (1 M) solution of the PbI2 in N,N−dimethylformamide (DMF) kept at 70 C.

The use of such a high PbI2 concentration is critical to obtaining the high loading of the mesoporous TiO2 films required to fabricate solar cells of the highest performance.

Further experimental details are provided in Method.

この部分の単語などは:

We prepared…　を準備した
spin-coating a solution　スピンを塗付した溶液
onto a compact underlayer　小さな下層に向けて　（The underlayer…　同じ言葉の使用はやめるべき）
acting as the electric front contact　電気的な表面層に対して
lead iodide　窯化鉛　[led]と発音する
1M solution　濃度１モルの溶液
a high concentration **is crucial**　濃い濃度は絶対に必要である
fabricate solar cells of the highest performance　最高の効率をもつ太陽電池を製造する
Further experimental details are provided in…　より詳細な実験法は…を参照してほしい

（訳文）
30nm 厚さの TiO2 層に向けスピン塗付したコロイドのアナターゼ粒子の溶液を
メソ孔の TiO2（アナターゼ）フィルムとして準備した。

下層はエアロゾルをスプレーした熱分解物を透明な導電性酸素のガラス基層として，
太陽セルの電気的前側の接触として，堆積させる。

そして2価ヨウ素鉛は TiO2 のナノ孔として，462mg/ml(濃度 1 モル)を持つ摂氏 70 度の
DMF の PbI2 溶液として用意した。

この高密度である PbI2 溶液の使用は，きわめて高い効率で太陽セルを製造し，
高密度のメソ孔 TiO2 フィルムの生成のためには絶対必要である。

詳しい実験の詳細はメソッドの項に書いてある。

その後の段落の単語:
scanning electron microscopy(SEM)　走査型電子顕微鏡
thus-prepared film　そのように準備したフィルム
infiltration　浸透
, indicating the…　それが…を示している　-> 文意として，sentence で続けている
optical absorption emission　光学発光と吸収

➢ **Figure 1　英語と訳文**　（Figure では，主語で内容が分かるので，普通述語は書かない。）

Figure 1 | Transformation of PbI2 into CH3NH3PbI3 within the nanopores of a mesoscopic TiO2 film.

a, Cross-sectional SEM of a mesoporous TiO2 film infiltrated with PbI2. FTO, fluorine-doped tin oxide.
b, Change in absorbance at 550 nm of such a film monitored during the transformation.
c, Change in photoluminescence (PL) intensity at 520 nm monitored during the transformation. Excitation at 460 nm.
d, Change in photoluminescence intensity at 775 nm monitored during the transformation. Excitation at 660 nm.
e, X-ray diffraction spectra of PbI2 on glass and porous TiO2/glass before and after the transformation. The dipping time was 60 s in both cases. The plot shows the X-ray intensity as a function of 2h (twice the diffraction angle).

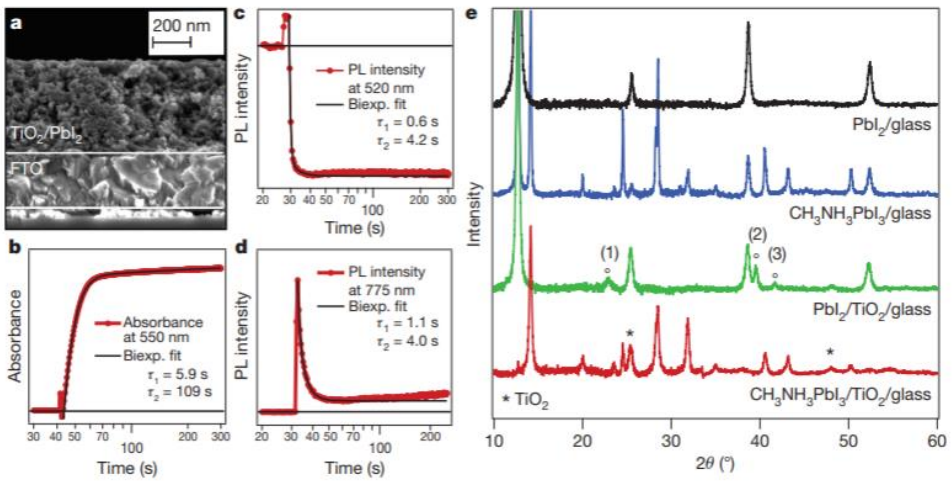

Figure 1　PbI2 から CH3NH3PbI3 へ向けたメソスケール TiO2 フィルムの変様

a.　メソ孔 TiO2 の SEM 像断面図で，透過した bI2, FTO，フッ素ドープした酸化 Ti
b.　変換中をモニターしたフィルムの 550 nm 吸収量の変化
c.　520 nm における変換中の光発光(PL)強度の変化。460 nm で励起の場合。
d.　775 nm の変換中の光発光強度の変化。660 nm で励起。
e.　変様の前と後でのガラスと孔あき TiO2/ガラスの PbI2 の X 線回折スペクトル。
どちらも漬ける時間は 60 秒。プロットは 2h（回折角度の 2 倍）の関数として X 線強度を示す。

Fig.1　**Caption**　（写真，図の）**説明文**
transformation　形の変容
photo luminescense　（冷たい）光発光

2 ページ左列の単語など

on the basis of literature data　文献データの根拠では　<- 基礎，がもとの意味
the PbI2 … crystallizes　主語＋動詞　これをすぐ把握することが大切！
the most common PbI2 modification　普通には，この句は which is…を補って始めている
grow in a preferential direction　優先の方向に成長する
along the c axis　c軸の方向に　<- a 軸に垂直な方向
hence the appearance of …　多くの場合，主語を省略する「帰結として…が現れる」
suggesting that the anatase scaffold induces for a different orientation
　（接続詞クローズとして追加で）：別の方向に成長することが考えられる

can **be attributed to …**　に帰せられる
is assigned to　に原因がある　<- be attribute と同じ
　a different PbI2 variant　ほかの Pbi2 の生成物（変種）
is beyond the scope of this report　このレポートの範囲を超えている

in striking contrast to the behavior of …　の振る舞いに**大きな違い**を
the conversion … is practically complete　（主語＋動詞）変換の様子は実際は完璧である
　as **is evidenced from** the immediate disappearance … and the concomitant appearance
　　直ちに消滅すること，および付随しての出現…が立証している
Notably,…　明白であるように
　confining the PbI2 crystals … drastically enhances　（主語，動詞）大きく増加している
, which **is complete** within a few seconds **of their coming** into contact
　　そして，数秒で完成する　　接触すること<- 動名詞
　　<- ほぼ文章をブロック is complete で理解し，そして次 of their coming…へ続く

larger PbI2 crystallites … are formed, resulting in …　大きな結晶が起き，それで…が結果である
show that the perovskite … adopts a morphology　形態を取り入れる　<- 主語，動詞

A key finding of the present work is that …　現在の仕事の大切な発見は，…である
　the PbI2 … greatly facilitates …　（主語＋動詞）
　　facilitate　容易にしている　<- 何度も出てくる表現！
that **are** not easily, or not at all, **accessible by**
　あまり易しくない，あるいは不可能でなくても，…で入手（or　理解）することを
dispersed II-V semiconductor　いくつかの II-V 種のセミコンダクター（半導体）
　2 族　3d 電子の遷移金属　原子量　Ti 22　Fe 26　Cu 29
　　4d　　Cd 48
　3 族　Ga 31　In 49
　15 族　As 33　Sb 51　高効率では，太陽電池は III-V 種が多い

while preserving particle size and　-> 粒子径…などは同じとして…
the thermodynamic driving force of such a reaction　反応などの熱力学を推進する力（働き）
bulk lattice energy　格子間の実際のエネルギー
serves as **a template** for …　の金型としてはたらく（機能している）
desired compound　望ましい混合物質
the insertion of the organic **cation**　有機物**正イオン**の挿入物
anion　負イオン

➢ 2 ページ右列, 19 行目から

Numerous literature reports show that … <- 主語＋動詞, that で始まるフレーズ
strong intralayer chemical bonding, as…interactions, allows the easy insertion of guest molecules
強い層間の化学結合が… ゲスト分子が容易に挿入されることを可能にしている
as… : 極めて弱いレイヤー間の van der Waals 相互作用を含めて

In our case, the large energy… , **combined with…, which… kinetics,** finally **enables** the transformation to be completed within seconds
（あいだが 2 つの長い文章がはさまれている。本来はカッコ書きか，複数の文にすべき！）
大きなエネルギーが … 数秒で完結する変換を起こしている（可能としている）

➢ **2 ページ右列中段 英語と訳文：ここが実験結果の核心**

In our case, **the large energy of formation of the hybrid perovskite,** combined with the nanoscopic morphology of the PbI2 precursor, which greatly enhances the reaction kinetics, finally **enables the transformation** to be completed within seconds

We used the sequential deposition technique to fabricate mesoscopic solar cells employing the triarylamine derivative 2,29,7,79-tetrakis(N,N-di-p-methoxyphenylamine)-9,99-spirobifluorene (spiro-MeOTAD) (Supplementary Fig. 2) as a hole-transporting material (HTM).

We note that, following a recently reported concept[25], **we use a Co(III) complex** as a p-type dopant for the HTM at a molar doping level of 10% to ensure a sufficient conductivity and low series resistance.

Figure 2 shows a crosssectional SEM picture of a typical device.

The mesoporous TiO2 film had an optimized thickness of around 350 nm and was infiltrated with the perovskite nanocrystals using the above-mentioned two-step procedure.

The HTM was subsequently deposited by spin coating. **It penetrates** into the remaining available pore volume and forms a 100-nm-thick layer on top of the composite structure.

A thin gold layer was thermally evaporated under vacuum onto the HTM, forming the back contact of the device.

単語などは:

as a hole-transportation material (HTM) ホール（正孔）輸送の物質
a Co(III) complex as a p-type dopant for the HTM p型タイプのドーパントとしての Co 原子複合体
半導体にドーピング（微量添加）される不純物。p 型またはn型半導体が作られる
at a molar doping level of 10% モル比の微量添加で 10%の
<- モル比で 10%レベルはかなり量が多い !!

was infiltrated … using **the above-mentioned two-step procedure**s
浸透させる **以前に述べた** <- よく使う言葉

（訳文）

我われの場合，混合ペロブスカイトの大きな生成エネルギーは，PbI2 前駆体のナノスケール形態論と大きな反応運動論が加速して，最後に数秒で終わる変換で完了する。

我われは連続変性法で，メソスコピックな太陽電池セルをホール輸送物質(HTM)である
トリアリールアミン融通体…フッ素（補足 Fig.2）を使うことで製造した。

最近報告されたコンセプトに従い， p 型ドーパントとして，十分な通電性で低抵抗
を確認できる HTM がモル比でドープレベルの 10%で働く 3 価の Co 複合体を使った。

Figure 2 は典型的な断面投影 SEM 像を示す

メソ孔 TiO2 フィルムは最適化した厚みの 350nm を用い，上で述べた
2 段階法を用いたペロブスカイトのナノ結晶を浸透させた。

HTM はそれからスピンコーティングで析出させた。それは残りの孔の体積に
広げて，100nm 厚さの層を形成した。

薄い金層は HTM へ向け，熱的に真空に蒸発させ，デバイスの裏面コンタクトとした。

➢ 2 ページ右列下 英語と訳文

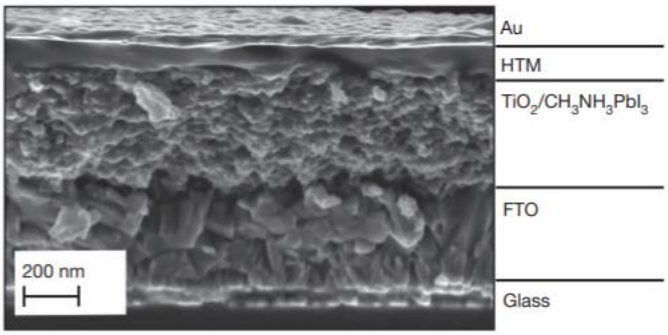

Figure 2 | **Cross-sectional SEM** of a complete photovoltaic device. Note that the thin TiO2 compact layer present between the FTO and the mesoscopic composite is not resolved in the SEM image.

It penetrates into the … pore volume　HTM は残りの孔領域の全体積を満たす
a layer **on top of** the composite structure　混成構造の部分を含めて
was thermally evaporated　熱的に**蒸着した**
back contact　裏面コンタクト（処理，接点）

（訳文）
全体の光起電力デバイスの SEM 像断面写真。FTO とメソスケールコンポジットの
薄い TiO2 層は SEM イメージでは解像度不足で解析できない。

➢　ここより実験測定を述べている

solar cell　太陽電池**セル**　<-「セル」が話題の中心である
under simulated air mass … and in the dark　模擬した air mass および暗部実験において
　the short-circuit **photocurrent**　短絡した光電流　17 mA/cm2
　the open-circuit **voltage**　短絡した電圧　992 mV
　the **fill factor**, respectively,　充填ファクター　0.73
　　<- 2 つ以上の項目を並べるときは，respectively を前（または後ろ）に書く（鉄則！）

>> この論文のセールスポイント

　yielding a solar-to-electric power conversion efficiency (PCE) 12.9%
　　太陽―電界のパワー変換効率(PCE)は 12.9%を得ている
　statistical data　統計的データ　<- ここに横に並べている

接続詞がなしで（口語的な表現）
　…, **we infer that** photovoltaics with … can be realized　光起電力…が実現されると推測する

➢　3ページ左列上から

incident-photon-to-current conversion efficiency　光入射と電流への変換効率
external quantum efficiency　外部の量子効率
Generation of photocurrent starts at 800 nm, in agreement with the bandgap of the CH3NH3PbI3
　　800 nm の光電流が発生することは，CH3NH3PbI3 のバンドギャップと一致して
is negligibly small　無視できるほど小さい
reveals that the value … result from …　（主語＋動詞）と一致している
the **smaller** absorption of　より小さく減衰していく　-> 実際，絵をみるとそうなっている

absorbed-photon-to-current conversion efficiency　吸収光子と電流**への変換効率**
　　->物理的に，「**大きな振動数　＝　短い波長**」に対応している

Detailed data can be found…　このデータは…を参照してほしい　<- 決まった表現
benefit from　で恩恵を受けている，つまり，良い結果を得ている
improving the…　（それで）改善されている…
is likely to result from…　から帰結される可能性がある
inducing the growth of larger crystals…　を誘発している　<- that induces the…と文章で書くべきところ
are ongoing　進行中である（英語的な言い方）

➢ Figure 3　英語と訳文:

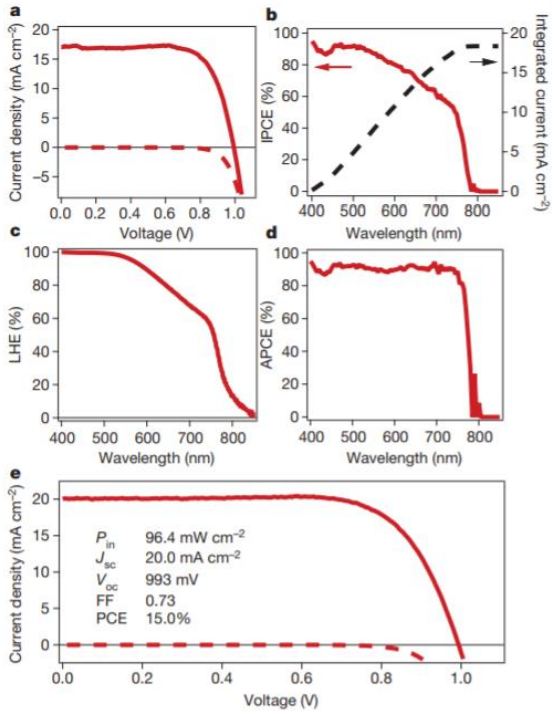

Figure 3 | **Photovoltaic device characterization.**

a, **J–V curves** for a photovoltaic device measured at a simulated AM1.5G solar irradiation of 95.6 mW cm^{-2} (solid line) and in the dark (dashed line).

b, **IPCE spectrum. The right-hand axis indicates** the integrated photocurrent that is expected to be generated under AM1.5G irradiation.

c, **LHE spectrum.**
d, **APCE spectrum** derived from the IPCE and LHE.

e, **J–V curves** for a best-performing cell measured at a simulated AM1.5G solar irradiation of 96.4 mW cm2 (solid line) and in the dark (dashed line). **The device was fabricated** using slightly modified deposition conditions (Methods). FF, fill factor.

（訳文）
光電圧デバイスの特性

a.　シミュレートした AM1.5G 太陽光放射 95.6 mV/cm2（太線）と暗電流（ダッシュ線）に対する放射光電圧デバイスの電流-電圧曲線

b.　IPCE スペクトル。右側の座標軸は，AM1.5G 放射のもと生成されると予想される積分した光電流を示す

c.　LHE スペクトル
d.　IPCE および LHE で導いた APCE スペクトル

e.　シミュレートした AM1.5G 太陽光放射 96.4 mV/cm2（太線）と暗電流（ダッシュ線）に対して最高記録のセルに対する電流-電圧曲線。このデバイスでは少し異なる変性法（Method），FF，充填因子で製造した。

Table 1: Photovoltaics performance at different light intensities
Intensity(mW cm2 Jsc (mA cm2) Voc (mV) Fill factor PCE (%)

様々の光強度に対する光起電力の効率
強度　最大電流　最大電圧　充填因子　PCE

➢ **3 ページ右列，最後の段落　英語と訳文　　結論部分**
論文の結論を締めくくる。

The sequential deposition method for the fabrication of perovskite-sensitized mesoscopic solar cells introduced here provides a means to achieve excellent photovoltaic performance with high reproducibility.

The power conversion efficiency of 15% achieved with the best device **is amongst the highest** for solution-processed photovoltaics and **sets a new record** for organic or hybrid inorganic-organic solar cells in general.

Our findings open new routes for the fabrication of perovskite-based photovoltaic devices, because other performed metal halide mesostructures may be converted into the desired perovskite by the simple insertion reaction detailed here.

On the basis of our results, **we believe** **that** **this new class** of mesoscopic solar cells **will find** widespread applications and **will eventually lead** to devices that rivals conventional silicon-based photovoltaics.

（訳文）
ペロブスカイト色素増感のメソスケール太陽電池セルを製作する連続変性法は
高い再現性をもつ素晴らしい光起電力の効率を達成する方法を与えている。

デバイスにて得られた 15%のパワー変換効率は，
溶液プロセスの光起電力で最高の値であり，
有機または無機有機混合の太陽電池セルで新記録といえる。

私たちの発見はペロブスカイト起源の光起電力装置の方法に新しい道を開いている。

その理由として，他の金属ハロゲンのメソ構造が，簡単な中間反応により望む
ペロブスカイトに変換すると考えており，また
既存シリコンベースの光起電力と並ぶデバイスに連なるものと確信する。

Sequential deposition as a route to high–performance perovskite–sensitized solar cells

Julian Burschka[1]*, Norman Pellet[1,2]*, Soo-Jin Moon[1], Robin Humphry-Baker[1], Peng Gao[1], Mohammad K. Nazeeruddin[1] & Michael Grätzel[1]

Following pioneering work[1], solution-processable organic–inorganic hybrid perovskites—such as $CH_3NH_3PbX_3$ (X = Cl, Br, I)—have attracted attention as light-harvesting materials for mesoscopic solar cells[2–15]. So far, the perovskite pigment has been deposited in a single step onto mesoporous metal oxide films using a mixture of PbX_2 and CH_3NH_3X in a common solvent. However, the uncontrolled precipitation of the perovskite produces large morphological variations, resulting in a wide spread of photovoltaic performance in the resulting devices, which hampers the prospects for practical applications. Here we describe a sequential deposition method for the formation of the perovskite pigment within the porous metal oxide film. PbI_2 is first introduced from solution into a nanoporous titanium dioxide film and subsequently transformed into the perovskite by exposing it to a solution of CH_3NH_3I. We find that the conversion occurs within the nanoporous host as soon as the two components come into contact, permitting much better control over the perovskite morphology than is possible with the previously employed route. Using this technique for the fabrication of solid-state mesoscopic solar cells greatly increases the reproducibility of their performance and allows us to achieve a power conversion efficiency of approximately 15 per cent (measured under standard AM1.5G test conditions on solar zenith angle, solar light intensity and cell temperature). This two-step method should provide new opportunities for the fabrication of solution-processed photovoltaic cells with unprecedented power conversion efficiencies and high stability equal to or even greater than those of today's best thin-film photovoltaic devices.

We prepared mesoporous TiO_2 (anatase) films by spin-coating a solution of colloidal anatase particles onto a 30-nm-thick compact TiO_2 underlayer. The underlayer was deposited by aerosol spray pyrolysis on a transparent-conducting-oxide-coated glass substrate acting as the electric front contact of the solar cell. Lead iodide (PbI_2) was then introduced into the TiO_2 nanopores by spin-coating a 462 mg ml^{-1} (~1 M) solution of PbI_2 in *N*,*N*-dimethylformamide (DMF) kept at 70 °C. The use of such a high PbI_2 concentration is critical to obtaining the high loading of the mesoporous TiO_2 films required to fabricate solar cells of the highest performance. Further experimental details are provided in Methods.

Figure 1a presents a cross-sectional scanning electron microscopy (SEM) image of the thus-prepared film. The absence of any PbI_2 crystals protruding from the surface of the mesoporous anatase layer shows that our infiltration method leads to a structure in which the PbI_2 is entirely contained within the nanopores of the TiO_2 film.

Dipping the TiO_2/PbI_2 composite film into a solution of CH_3NH_3I in 2-propanol (10 mg ml^{-1}) changes its colour immediately from yellow to dark brown, indicating the formation of $CH_3NH_3PbI_3$. We monitored the dynamics of the formation of the perovskite by optical absorption, emission and X-ray diffraction (XRD) spectroscopy. Figure 1b shows that the increase over time of the perovskite absorption at 550 nm is

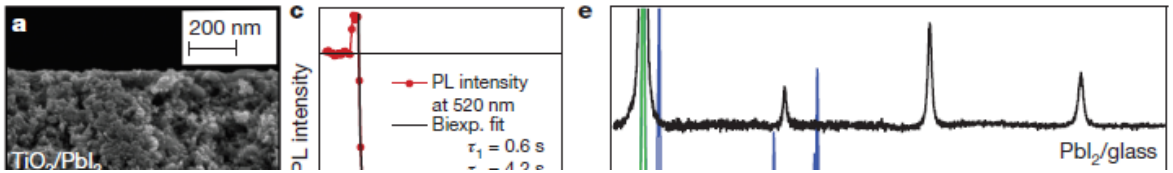

to achieve a power conversion efficiency of approximately 15 per cent (measured under standard AM1.5G test conditions on solar zenith angle, solar light intensity and cell temperature). This two-step method should provide new opportunities for the fabrication of solution-processed photovoltaic cells with unprecedented power

2-propanol (10 mg ml^{-1}) changes its colour immediately from yellow to dark brown, indicating the formation of $CH_3NH_3PbI_3$. We monitored the dynamics of the formation of the perovskite by optical absorption, emission and X-ray diffraction (XRD) spectroscopy. Figure 1b shows that the increase over time of the perovskite absorption at 550 nm is

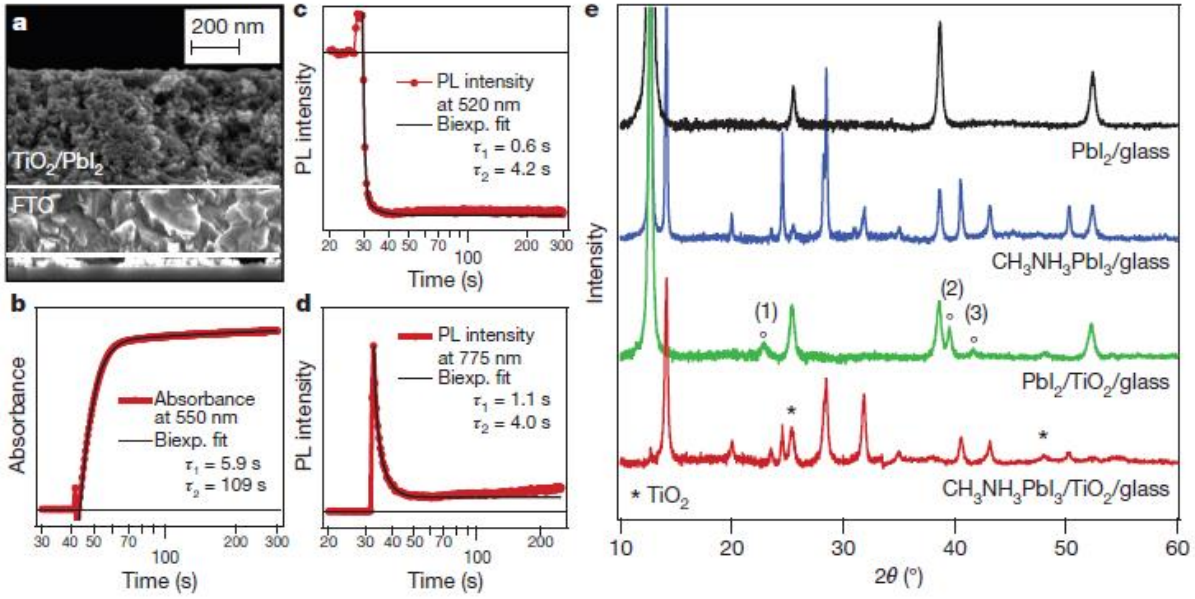

Figure 1 | Transformation of PbI_2 into $CH_3NH_3PbI_3$ within the nanopores of a mesoscopic TiO_2 film. **a**, Cross-sectional SEM of a mesoporous TiO_2 film infiltrated with PbI_2. FTO, fluorine-doped tin oxide. **b**, Change in absorbance at 550 nm of such a film monitored during the transformation. **c**, Change in photoluminescence (PL) intensity at 520 nm monitored during the transformation. Excitation at 460 nm. **d**, Change in photoluminescence intensity at 775 nm monitored during the transformation. Excitation at 660 nm. **e**, X-ray diffraction spectra of PbI_2 on glass and porous TiO_2/glass before and after the transformation. The dipping time was 60 s in both cases. The plot shows the X-ray intensity as a function of 2θ (twice the diffraction angle).

[1]Laboratory of Photonics and Interfaces, Department of Chemistry and Chemical Engineering, Swiss Federal Institute of Technology, Station 6, CH-1015 Lausanne, Switzerland. [2]Max-Planck-Institute for Solid-State Research, Heisenbergstraße 1, D-70569 Stuttgart, Germany.
*These authors contributed equally to this work.

practically complete within a few seconds of exposing the PbI_2-loaded TiO_2 film to the CH_3NH_3I solution. A small additional increase in the absorbance, occurring on a timescale of 100 s and contributing only a few per cent to the total increase of the signal, is attributed to morphological changes producing enhanced light scattering. The conversion is accompanied by a quenching of the PbI_2 emission at 425 nm (Fig. 1c) and a concomitant increase in the perovskite luminescence at 775 nm (Fig. 1d). The latter emission passes through a maximum before decreasing to a stationary value. This decrease results from self-absorption of the luminescence by the perovskite formed during the reaction with CH_3NH_3I. The traces were fitted to a biexponential function yielding the decay times stated in Fig. 1b–d. We note that the increase in the emission intensity before the quenching in Fig. 1c is an optical artefact that results from opening the sample compartment to add the CH_3NH_3I solution.

The green and red curves in Fig. 1e show X-ray powder diffraction spectra measured before and, respectively, after the TiO_2/PbI_2 nanocomposite film is brought into contact with the CH_3NH_3I solution. For comparison, we spin-coated the PbI_2 also on a flat glass substrate and exposed the resulting film to a CH_3NH_3I solution in the same manner as the TiO_2/PbI_2 nanocomposite. On the basis of literature data, the PbI_2 deposited by spin-coating from DMF solution crystallizes in the form of the hexagonal 2H polytype, the most common PbI_2 modification (Inorganic Crystal Structure Database, collection code 68819; http://www.fiz-karlsruhe.com/icsd.html). Moreover, the results show that on a flat glass substrate, crystals grow in a preferential orientation along the *c* axis, hence the appearance of only four diffraction peaks, corresponding to the (001), (002), (003) and (004) lattice planes (Fig. 1e, black curve). For the PbI_2 loaded on a mesoporous TiO_2 film (Fig. 1e, green curve), we find three additional diffraction peaks that do not originate from TiO_2, suggesting that the anatase scaffold induces a different orientation for the PbI_2 crystal growth. The peaks labelled (2) and (3) in Fig. 1e can be attributed to the (110) and (111) lattice planes of the 2H polytype. Peak (1) is assigned to a different PbI_2 variant, whose identification is beyond the scope of this report in view of the large number of polytypes that have been reported for PbI_2 (ref. 16).

During the reaction with CH_3NH_3I, we observe the appearance of a wide range of sizes are formed when the perovskite is deposited in a single step from a solution of CH_3NH_3I and PbI_2 in γ-butyrolactone or DMF.

A key finding of the present work is that the confinement of the PbI_2 within the nanoporous network of the TiO_2 film greatly facilitates its conversion to the perovskite pigment. Moreover, the mesoporous scaffold of the host forces the perovskite to adopt a confined nanomorphology.

The literature contains several examples in which a two-step procedure is used to fabricate nanostructures that are not easily, or not at all, accessible by a direct synthetic route. Ion exchange reactions have, for example, been used to convert dispersed II–V semiconductor nanocrystals into the corresponding III–V analogues while preserving particle size and distribution as well as the initial nanomorphology[19–21]. As reported, the thermodynamic driving force of such a reaction is the difference in bulk lattice energy for the two materials, and the initial crystal lattice serves as a template for the formation of the desired compound. As for PbI_2, the insertion of the organic cation is facilitated through the layered PbI_2 structure, which consists of three spatially repeating planes, I–Pb–I (ref. 16). Numerous literature reports show that strong intralayer chemical bonding, as well as only weak interlayer van der Waals interactions, allows the easy insertion of guest molecules between these layers[22–24]. In our case, the large energy of formation of the hybrid perovskite, combined with the nanoscopic morphology of the PbI_2 precursor, which greatly enhances the reaction kinetics, finally enables the transformation to be completed within seconds.

We used the sequential deposition technique to fabricate mesoscopic solar cells employing the triarylamine derivative 2,2′,7,7′-tetrakis(*N*,*N*-di-*p*-methoxyphenylamine)-9,9′-spirobifluorene (spiro-MeOTAD) (Supplementary Fig. 2) as a hole-transporting material (HTM). We note that, following a recently reported concept[25], we use a Co(III) complex as a p-type dopant for the HTM at a molar doping level of 10% to ensure a sufficient conductivity and low series resistance. Figure 2 shows a cross-sectional SEM picture of a typical device. The mesoporous TiO_2 film had an optimized thickness of around 350 nm and was infiltrated with the perovskite nanocrystals using the above-mentioned two-step procedure. The HTM was subsequently deposited by spin coating. It penetrates into the remaining available pore volume and forms a 100-nm-thick layer on

and (3) in Fig. 1e can be attributed to the (110) and (111) lattice planes of the 2H polytype. Peak (1) is assigned to a different PbI_2 variant, whose identification is beyond the scope of this report in view of the large number of polytypes that have been reported for PbI_2 (ref. 16).

During the reaction with CH_3NH_3I, we observe the appearance of a series of new diffraction peaks that are in good agreement with literature data on the tetragonal phase of the $CH_3NH_3PbI_3$ perovskite[17]. However, when PbI_2 is deposited on a flat film (Fig. 1e, blue curve) the conversion to perovskite on exposure to the CH_3NH_3I solution is incomplete; a large amount of unreacted PbI_2 remained even after a dipping time of 45 min. This agrees with the observation that the CH_3NH_3I insertion hardly proceeds beyond the surface of thin PbI_2 films, and that the complete transformation of the crystal structure requires several hours[18]. A caveat associated with such long conversion times is that the perovskite dissolves in the methylammonium iodide solution over longer periods, hampering the transformation.

In striking contrast to the behaviour of thin films of PbI_2 deposited on a flat support, the conversion of PbI_2 nanocrystals in the mesoporous TiO_2 film is practically complete on a timescale of seconds, as is evident from the immediate disappearance of its most intense diffraction peak (the (001) peak) and the concomitant appearance of the XRD reflections for the tetragonal perovskite. When the PbI_2 crystals are contained within the mesoporous TiO_2 scaffold, their size is limited to ~22 nm by the pore size of the host. Notably, we find that confining the PbI_2 crystals to such a small size drastically enhances their rate of conversion to perovskite, which is complete within a few seconds of their coming into contact with the methylammonium iodide solution. However, when deposited on a flat surface, larger PbI_2 crystallites in the size range of 50–200 nm are formed, resulting in incomplete conversion of the PbI_2 on exposure to CH_3NH_3I, as shown by XRD. The SEM images of such a film that are depicted in Supplementary Fig. 1e, f show, however, that the perovskite produced by the sequential deposition technique adopts a morphology similar to that of the PbI_2 precursor. Supplementary Fig. 1 also shows that large crystals of $CH_3NH_3PbI_3$ with a sectional SEM picture of a typical device. The mesoporous TiO_2 film had an optimized thickness of around 350 nm and was infiltrated with the perovskite nanocrystals using the above-mentioned two-step procedure. The HTM was subsequently deposited by spin coating. It penetrates into the remaining available pore volume and forms a 100-nm-thick layer on top of the composite structure. A thin gold layer was thermally evaporated under vacuum onto the HTM, forming the back contact of the device.

We measured the current density (J)–voltage (V) characteristics of the solar cells under simulated air mass 1.5 global (AM1.5G) solar irradiation and in the dark. Figure 3a shows J–V curves measured at a light intensity of 95.6 mW cm^{-2} for a typical device. From this, we derive values for the short-circuit photocurrent (J_{sc}), the open-circuit voltage (V_{oc}) and the fill factor of, respectively, 17.1 mA cm^{-2}, 992 mV and 0.73, yielding a solar-to-electric power conversion efficiency (PCE) of 12.9% (Table 1). Statistical data on a larger batch of ten photovoltaic devices is shown in Supplementary Table 1. From the

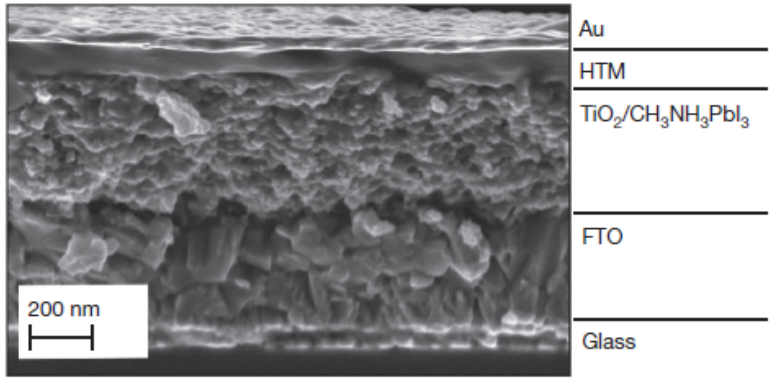

Figure 2 | Cross-sectional SEM of a complete photovoltaic device. Note that the thin TiO_2 compact layer present between the FTO and the mesoscopic composite is not resolved in the SEM image.

average PCE value of 12.0% ± 0.5% and the small standard deviation, we infer that photovoltaics with excellent performance and high reproducibility can be realized using the method reported here.

Figure 3b shows the incident-photon-to-current conversion efficiency (IPCE), or external quantum efficiency, spectrum for the perovskite cell. Generation of photocurrent starts at 800 nm, in agreement with the bandgap of the $CH_3NH_3PbI_3$, and reaches peak values of over 90% in the short-wavelength region of the visible spectrum. Integrating the overlap of the IPCE spectrum with the AM1.5G solar photon flux yields a current density of 18.4 mA cm^{-2}, which is in excellent agreement with the measured photocurrent density, extrapolated to 17.9 mA cm^{-2} at the standard solar AM1.5G intensity of 100 mW cm^{-2}. This confirms that any mismatch between the simulated sunlight and the AM1.5G standard is negligibly small. Comparison with the absorptance or light-harvesting efficiency (LHE) depicted in Fig. 3c reveals that the low IPCE values in the range of 600–800 nm result from the smaller absorption of the perovskite in this spectral region. This is also reflected in the spectrum of the internal quantum efficiency, or absorbed-photon-to-current conversion efficiency (APCE), which can be derived from the IPCE and LHE and is shown in Fig. 3d. The APCE is greater than 90% over the whole visible region, without correction for reflective losses, indicating that the device achieves near-unity quantum yield for the generation and collection of charge carriers.

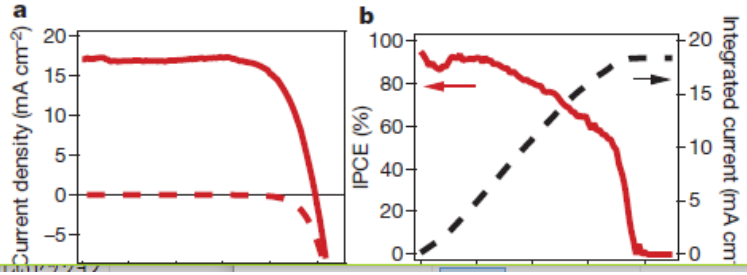

Table 1 | Photovoltaics performance at different light intensities

Intensity (mW cm^{-2})	J_{sc} (mA cm^{-2})	V_{oc} (mV)	Fill factor	PCE (%)
9.3	1.7	901	0.77	12.6
49.8	8.9	973	0.75	13.0
95.6	17.1	992	0.73	12.9

In an attempt to increase the loading of the perovskite absorber on the TiO_2 structure and to obviate the lack of absorption in the long-wavelength region of the spectrum, we slightly modified the conditions for the deposition of the PbI_2 precursor as well as the transformation reaction. Details are provided in Methods. The *J*–*V* characteristics of the best-performing cell of the series that was fabricated in this manner are depicted in Fig. 3e. From this data, we derive values of 20.0 mA cm^{-2}, 993 mV and 0.73 for J_{sc}, V_{oc} and the fill factor, respectively, yielding a PCE of 15.0% measured at a light intensity of P_{in} = 96.4 mW cm^{-2}. To the best of our knowledge, this is the highest power conversion efficiency reported so far for organic or hybrid inorganic–organic solar cells and one of the highest for any solution-processed photovoltaic device. Several solar cells with PCEs between 14% and 15% were fabricated. One of these devices was sent to an accredited photovoltaic calibration laboratory for certification, confirming a power conversion efficiency of 14.14% measured under standard AM1.5G reporting conditions. Detailed photovoltaics data for this device can be found in Supplementary Fig. 3. Compared with the devices from which we took the data shown in Fig. 3a and Supplementary Table 1, these top-performance devices benefit from a significantly higher photocurrent. We attribute this trend to the increased loading of the porous TiO_2 film with the perovskite pigment and to increased light scattering, improving the long-wavelength response of the cell. The increase in light scattering is likely to result from the additional pre-wetting step that was used for the top-performance devices. The pre-wetting locally decreases the methylammonium iodide concentration, inducing the growth of larger crystals. Detailed studies that aim to identify the key role of the different parameters

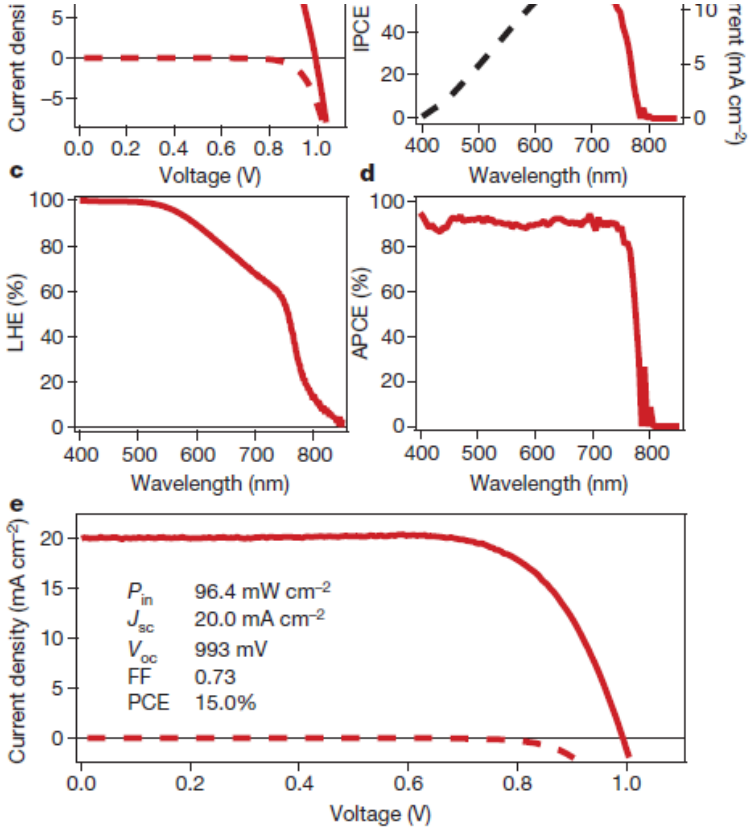

Figure 3 | Photovoltaic device characterization. **a**, *J*–*V* curves for a photovoltaic device measured at a simulated AM1.5G solar irradiation of 95.6 mW cm^{-2} (solid line) and in the dark (dashed line). **b**, IPCE spectrum. The right-hand axis indicates the integrated photocurrent that is expected to be generated under AM1.5G irradiation. **c**, LHE spectrum. **d**, APCE spectrum derived from the IPCE and LHE. **e**, *J*–*V* curves for a best-performing cell measured at a simulated AM1.5G solar irradiation of 96.4 mW cm^{-2} (solid line) and in the dark (dashed line). The device was fabricated using slightly modified deposition conditions (Methods). FF, fill factor.

the additional pre-wetting step that was used for the top-performance devices. The pre-wetting locally decreases the methylammonium iodide concentration, inducing the growth of larger crystals. Detailed studies that aim to identify the key role of the different parameters during the sequential deposition are ongoing.

To test the stability of the perovskite-based photovoltaics prepared using the aforementioned procedure, we subjected a sealed cell to long-term light soaking at a light intensity of ~100 mW cm^{-2} and a temperature of 45 °C. The device was encapsulated under argon and maintained at the optimal electric power output during the ageing using maximum-power-point tracking. We found a very promising long-term stability: the photovoltaic device maintained more than 80% of its initial PCE after a period of 500 h (Supplementary Fig. 4). Also, it is notable that we do not observe any change in the short-circuit photocurrent, indicating that there is no photodegradation of the perovskite light harvester. The decrease in PCE is therefore due only to a decrease in both the open-circuit potential and the fill factor, and the similar shape of the two decays suggests that they are linked to the same degradation mechanism. The change in these two parameters is mainly due to a decrease in the shunt resistance, as is apparent from Supplementary Fig. 5, where *J*–*V* curves of the device before and after the ageing process are shown.

The sequential deposition method for the fabrication of perovskite-sensitized mesoscopic solar cells introduced here provides a means to achieve excellent photovoltaic performance with high reproducibility. The power conversion efficiency of 15% achieved with the best device is amongst the highest for solution-processed photovoltaics and sets a new record for organic or hybrid inorganic–organic solar cells in general. Our findings open new routes for the fabrication of perovskite-based photovoltaic devices, because other preformed metal halide mesostructures may be converted into the desired perovskite by the simple insertion reaction detailed here. On the basis of our results, we believe that this new class of mesoscopic solar cells will find widespread application and will eventually lead to devices that rival conventional silicon-based photovoltaics.